J|A|C|S
ARTICLES

Published on Web 12/08/2010

Self-Assembled Quantum Dot-Sensitized Multivalent DNA Photonic Wires

Kelly Boeneman,[†] Duane E. Prasuhn,[†] Juan B. Blanco-Canosa,[‡] Philip E. Dawson,[‡] Joseph S. Melinger,[§] Mario Ancona,[§] Michael H. Stewart,[||] Kimihiro Susumu,[||] Alan Huston,[||] and Igor L. Medintz*,[†]

Center for Bio/Molecular Science and Engineering, Code 6900, Optical Sciences Division, Code 5611, and Electronic Science and Technology Division, Code 6800, U.S. Naval Research Laboratory, Washington, DC 20375, United States, and Departments of Cell Biology and Chemistry, The Scripps Research Institute, La Jolla, California 92037, United States

Received July 21, 2010; E-mail: Igor.medintz@nrl.navy.mil

Abstract: Combining the inherent scaffolding provided by DNA structure with spatial control over fluorophore positioning allows the creation of DNA-based photonic wires with the capacity to transfer excitation energy over distances greater than 150 Å. We demonstrate hybrid multifluorophore DNA−photonic wires that both self-assemble around semiconductor quantum dots (QDs) and exploit their unique photophysical properties. In this architecture, the QDs function as both central nanoscaffolds and ultraviolet energy harvesting donors that drive Förster resonance energy transfer (FRET) cascades through the DNA wires with emissions that approach the near-infrared. To assemble the wires, DNA fragments labeled with a series of increasingly red-shifted acceptor-dyes were hybridized in a predetermined linear arrangement to a complementary DNA template that was chemoselectively modified with a hexahistidine-appended peptide. The peptide portion facilitated metal-affinity coordination of multiple hybridized DNA−dye structures to a central QD completing the final nanocrystal−DNA photonic wire structure. We assembled several such hybrid structures where labeled-acceptor dyes were excited by the QDs and arranged to interact with each other via consecutive FRET processes. The inherently facile reconfiguration properties of this design allowed testing of alternate formats including the addition of an intercalating dye located in the template DNA or placement of multiple identical dye acceptors that engaged in homoFRET. Lastly, a photonic structure linking the central QD with multiple copies of DNA hybridized with 4-sequentially arranged acceptor dyes and demonstrating 4-consecutive energy transfer steps was examined. Step-by-step monitoring of energy transfer with both steady-state and time-resolved spectroscopy allowed efficiencies to be tracked through the structures and suggested that acceptor dye quantum yields are the predominant limiting factor. Integrating such DNA-based photonic structures with QDs can help create a new generation of biophotonic wire assemblies with widespread potential in nanotechnology.

Introduction

The unique chemical and scaffolding properties provided by double-stranded (ds) DNA structures have established them as building blocks for assembling and testing many new functional nanodevices.[1] In this context, their desirable characteristics include the ability to self-assemble into predictable helical structures of known, controlled length where placement of individual DNA fragments can be predetermined, the availability of automated synthetic methods to produce any desired sequence with multiple internal and terminal chemical modifications, and more recently, access to complex designer 2- and 3-D structures.[1−4] One area where DNA scaffolds have been intensively exploited is for assembling DNA-based photonic wire structures. These can be loosely defined as consisting of DNA scaffolds with a series of chromophores that display overlapping absorption/emission properties arranged on, or in, the DNA in a manner that allows them to interact.[4,5] Inherent DNA complementarity combined with mature labeling technologies now allow for routine placement of dyes at any point along an oligonucleotide strand along with control over the distances between interacting chromophores. Because of the spatial modulation and close confinement afforded by the DNA architecture, Förster resonance energy transfer (FRET) is the most common photophysical process exhibited by chromophores arranged in this manner. These structures can be engineered to enhance FRET via single or multiple energy transfer (ET) steps.[4,5] Although similar constructs have been demonstrated with protein and peptide scaffolds, these template materials are

[†] Center for Bio/Molecular Science and Engineering, Code 6900.
[‡] The Scripps Research Institute.
[§] Electronic Science and Technology Division, Code 6800.
[||] Optical Sciences Division, Code 5611.

(1) Lin, C.; Liu, Y.; Yan, H. *Biochemistry* **2009**, *48*, 1663–1674.
(2) Wood, J. *Mater. Today* **2006**, *9*, 9.
(3) Rothemund, P. W. K. *Nature* **2006**, *440*, 297–302.
(4) Varghese, R.; Wagenknecht, H. A. *Chem. Commun.* **2009**, *19*, 2615–2624.
(5) Hannestad, J. K.; Sandin, P.; Albinsson, B. *J. Am. Chem. Soc.* **2008**, *130*, 15889–15895.

harder to manipulate chemically and the same level of spatial control is not realizable.[6,7]

Multichromophore DNA-based photonic wires have undergone intense investigation with steady-state, time-resolved, and single-molecule fluorescence spectroscopy[8,9] for potential applications ranging from light harvesting antenna[10] and biological probes[11−13] to optical computing and switching devices.[14,15] This work has provided useful insights into the underlying mechanisms as well as important contributions to a broader array of research activities. For example, the Mathies group pioneered the use of DNA-based ET probes in genetic analysis which ultimately contributed to significantly facilitating the genomic sequencing revolution.[12,13] A series of structurally analogous FRET probes assembled on a DNA scaffold were synthesized where any one of 4 different acceptor fluorophores could optimally interact with a common donor molecule using a single laser excitation wavelength. Hannestad and co-workers recently engineered photonic wires capable of efficiently transporting excitation energy through the DNA structure.[5] Chromophores attached to opposite ends of a 50 base pair (bp) ds DNA, intralabeled with multiple copies of a YO-PRO-1 DNA intercalating dye, allowed multistep FRET migration over DNA lengths >20 nm. Other examples include fluorescently labeled oligodeoxyfluorosides for probing zebrafish embryos where the spacing of 1−4 constituent fluorophores provided emission maxima ranging from 376 to 633 nm.[16]

FRET-based photonic wires are inherently dependent on the photophysics of the fluorophores that are incorporated into their structures. Issues that limit the efficiency of energy transport can include pH-dependence, broad absorption, and emission spectra that lead to significant spectral cross-talk, low fluorescence quantum yields, susceptibility to photobleaching, and photodegradation.[17,18] The inclusion of robust fluorophores that overcome many of these issues could significantly contribute to improving the function of these structures. The size-dependent properties of semiconductor nanocrystals or quantum dots (QDs) have established them as versatile fluorophores for biological sensing, labeling, and imaging applications.[19−23] These same properties allow QDs to function as potent FRET donors with unique capabilities that are cumulatively unavailable to conventional organic dyes or protein fluorophores in the same role.[23] Pertinent characteristics include the ability to: controllably array multiple acceptors around a central QD which proportionally increases the probability of energy transfer by increasing the number of potential acceptors, select specific QD photoluminescence (PL) wavelengths to optimize spectral overlap with a given acceptor, excite the QD donor at a wavelength that corresponds to a minimum in the acceptor's absorbance, thus, reducing direct acceptor excitation, and access to multiphoton and multiplex FRET configurations.[23−25] A variety of FRET-based biosensors incorporating many of these properties have already been prototyped.[23]

Here we combine QDs with fluorophore-labeled DNA to create photonic wires with unique photophysical capabilities. DNA fragments prelabeled with acceptor-dyes were hybridized in a linearly ordered arrangement to a complementary DNA template chemoselectively modified with a hexahistidine-appended peptide. The hexahistidines facilitated self-assembly of multiple copies of hybridized DNA−dye to the QD completing the hybrid nanocrystal−DNA photonic wire, see schematic Figure 1. Within these structures, the QD fulfills several roles including central nanoscaffold and energy donor that drives multistep FRET cascades through the wires. The facile design reconfiguration allows several different QD-wire structures to be examined culminating in a QD linked to multiple copies of 4-linearly arranged donor/acceptor dyes.

Materials and Methods

Quantum Dots. CdSe−ZnS core−shell QDs with a PL maxima centered at ~530 nm (abbreviated as 530 nm QDs) were synthesized using a high temperature reaction of organometallic precursors in hot coordinating solvents.[26,27] QDs were made hydrophilic by exchanging the native capping shell with DHLA−PEG ligands where DHLA is a bidentate dihydrolipoic acid appended with polyethylene glycol (PEG) segments of MW ~750 that terminate in a methoxy group, see Supporting Information for the structure.[28,29]

DNA Sequences, Dye-Labeling, and Chemoselective Ligation to Modified Peptides. The DNA backbone and segments 1−4 (Figure 1B) were purchased from Operon Biotechnologies, Inc. (Huntsville, AL). Most were obtained with dye-acceptors inserted during synthesis along with identical unlabeled spacer (sp) segments of the same sequence. An amine modified T on DNA segment 4 was labeled with succinimidyl ester-activated Cy7 dye (GE Healthcare, Piscataway, NJ).[12] The 3′-aminated backbone DNA was covalently coupled to the 2-hydrazinonicotinoyl (HYNIC)-modified $(His)_6$-peptide using aniline-catalyzed chemoselective ligation.[30,31] The peptide sequence is given in Figure 1B. Briefly, aldehyde modified-DNA sequences were obtained by reacting ~0.45 mM

(6) Channon, K. J.; Devlin, G. L.; MacPhee, C. E. *J. Am. Chem. Soc.* **2009**, *131*, 12520–12521.
(7) Miller, R. A.; Presley, A. D.; Francis, M. B. *J. Am. Chem. Soc.* **2007**, *129*, 3104–3109.
(8) Heilemann, M.; Kasper, R.; Tinnefeld, P.; Sauer, M. *J. Am. Chem. Soc.* **2006**, *128*, 16864–16875.
(9) Heilemann, M.; Tinnefeld, P.; Mosteiro, G. S.; Parajo, M. G.; Van Hulst, N. F.; Sauer, M. *J. Am. Chem. Soc.* **2004**, *126*, 6514–6515.
(10) Ohya, Y.; Yabuki, K.; Hashimoto, M.; Nakajima, A.; Ouchi, T. *Bioconjugate Chem.* **2003**, *14*, 1057–1066.
(11) Tong, A. K.; Li, Z. M.; Jones, G. S.; Russo, J. J.; Ju, J. Y. *Nat. Biotechnol.* **2001**, *19*, 756–759.
(12) Berti, L.; Xie, J.; Medintz, I. L.; Glazer, A. N.; Mathies, R. A. *Anal. Biochem.* **2001**, *292*, 188–197.
(13) Ju, J. Y.; Glazer, A. N.; Mathies, R. A. *Nat. Med.* **1996**, *2*, 246–249.
(14) Vogelsang, J.; Cordes, T.; Tinnefeld, P. *Photochem. Photobiol. Sci.* **2009**, *8*, 486–496.
(15) Pistol, C.; Dwyer, C.; Lebeck, A. R. *IEEE Micro* **2008**, *28*, 7–19.
(16) Teo, Y. N.; Wilson, J. N.; Kool, E. T. *J. Am. Chem. Soc.* **2009**, *131*, 3923–3933.
(17) Lakowicz, J. R. *Principles of Fluorescence Spectroscopy*, 3 rd ed.; Springer: New York, 2006.
(18) Sapsford, K. E.; Berti, L.; Medintz, I. L. *Angew. Chem., Int. Ed.* **2006**, *45*, 4562–4588.
(19) Michalet, X.; Pinaud, F. F.; Bentolila, L. A.; Tsay, J. M.; Doose, S.; Li, J. J.; Sundaresan, G.; Wu, A. M.; Gambhir, S. S.; Weiss, S. *Science* **2005**, *307*, 538–544.
(20) Alivisatos, A. P.; Gu, W.; Larabell, C. A. *Ann. Rev. Biomed. Eng.* **2005**, *7*, 55–76.
(21) Klostranec, J. M.; Chan, W. C. W. *Adv. Mater.* **2006**, *18*, 1953–1964.
(22) Delehanty, J. B.; Mattoussi, H.; Medintz, I. L. *Anal. Bioanal. Chem.* **2009**, *393*, 1091–1105.
(23) Medintz, I. L.; Mattoussi, H. *Phys. Chem. Chem. Phys.* **2009**, *11*, 17–45.
(24) Clapp, A. R.; Medintz, I. L.; Uyeda, H. T.; Fisher, B. R.; Goldman, E. R.; Bawendi, M. G.; Mattoussi, H. *J. Am. Chem. Soc.* **2005**, *127*, 18212–18221.
(25) Clapp, A. R.; Medintz, I. L.; Mauro, J. M.; Fisher, B. R.; Bawendi, M. G.; Mattoussi, H. *J. Am. Chem. Soc.* **2004**, *126*, 301–310.
(26) Dabbousi, B. O.; Rodriguez-Viejo, J.; Mikulec, F. V.; Heine, J. R.; Mattoussi, H.; Ober, R.; Jensen, K. F.; Bawendi, M. G. *J. Phys. Chem. B.* **1997**, *101*, 9463–9475.
(27) Peng, Z. A.; Peng, X. *J. Am. Chem. Soc.* **2001**, *123*, 183–184.
(28) Mei, B. C.; Susumu, K.; Medintz, I. L.; Delehanty, J. B.; Mountziaris, T. J.; Mattoussi, H. *J. Mater. Chem.* **2008**, *18*, 4949–4958.
(29) Mei, B. C.; Susumu, K.; Medintz, I. L.; Mattoussi, H. *Nat. Protoc.* **2009**, *4*, 412–423.
(30) Dirksen, A.; Dawson, P. E. *Bioconjugate Chem.* **2008**, *19*, 2543–2548.

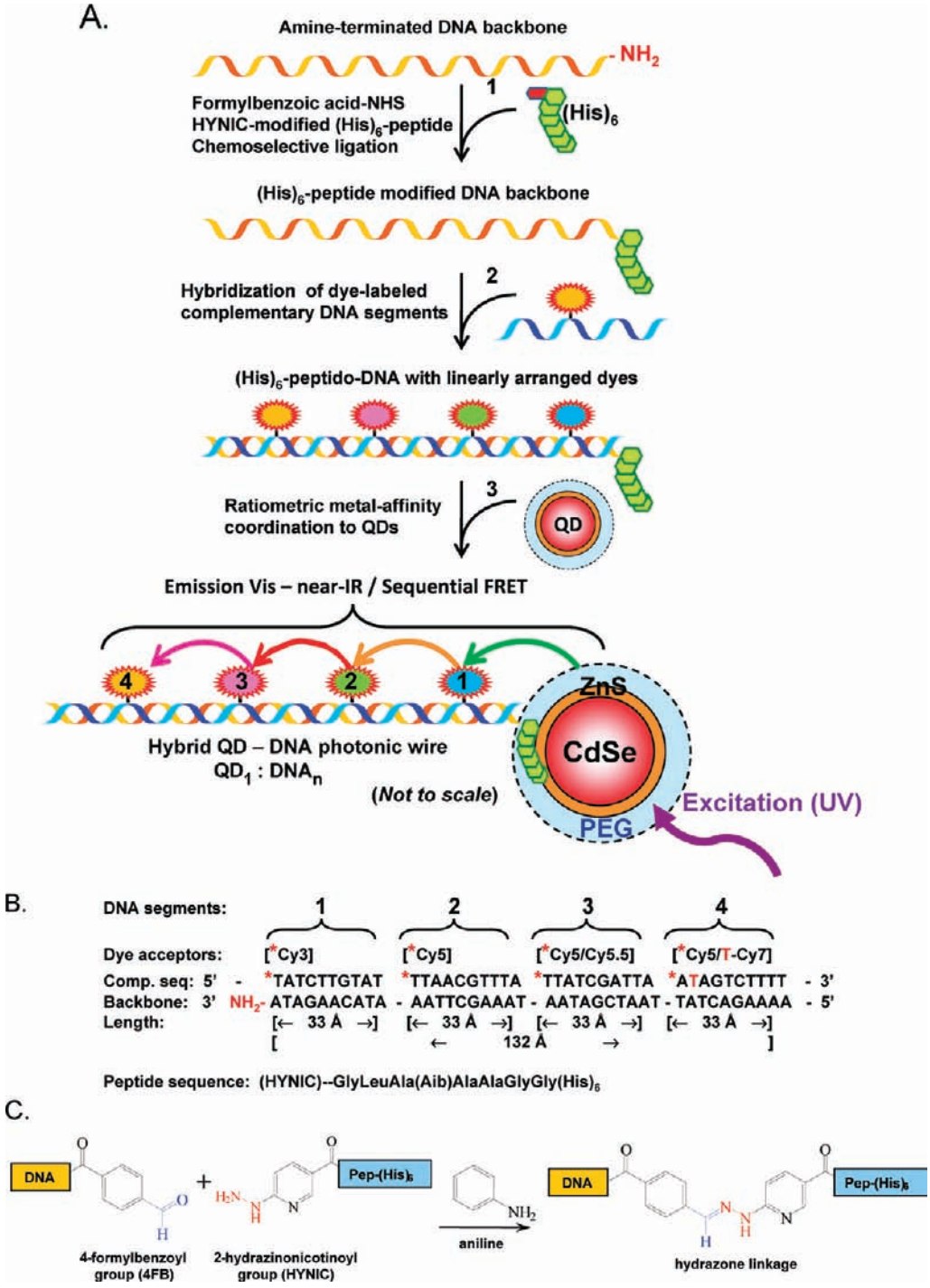

Figure 1. Schematic, DNA/peptide sequences, and peptide−DNA chemoselective ligation. (A) (1) The terminal amine group on the 'backbone' DNA is activated to a formylbenzoic acid and chemoselectively ligated to a HYNIC-modified $(His)_6$-peptide sequence. (2) Individual dye-labeled DNA strands are hybridized to their complementary sequence on the $(His)_6$-modified DNA backbone and (3) self-assembled to the QDs via metal-affinity coordination. The resulting structure consists of a central QD with multiple, rigid dye-labeled DNA centro-symmetrically arrayed on its surface as designated by the QD_1:DNA_n ratio. UV excitation of the system results in an energy transfer cascade from the central QD through the sequential aligned dye-acceptors which emit from the visible to the near IR portion of the spectrum. 1−4 indicate sequential dyes and are used to indicated dye position relative to the QD in subsequent experiments. (B) DNA sequences including the amine-functionalized DNA backbone and the 4 complementary segments which hybridize to it denoted as 1−4. Those particular positions on the DNA backbone also denoted as 1−4. The dye acceptors utilized with particular sequence are shown above each. Sequences purchased with a dye-acceptor incorporated during synthesis are designated by the red asterisk. The amine-modified T subsequently labeled with Cy7 is shown in red on segment 4. Estimated end-to-end lengths for each segment along with the overall structure are given along with the sequence of the HYNIC-modified $(His)_6$-peptide. Dye structures and selected DNA linker structures are shown in Supporting Figure 1. (C) Schematic of the aniline-catalyzed hydrazone ligation between aldehyde in blue and hydrazine functionalities in red utilized to join the DNA to the $(His)_6$-peptide.

amine-terminated DNA in 1× phosphate buffered saline pH 7.4 (PBS, 137 mM NaCl, 10 mM phosphate, and 2.7 mM KCl) with 9.09 mM *p*-formylbenzoic acid-*N*-hydroxysuccinimide ester (Sigma-Aldrich, Saint Louis, MO; 100 mM stock solution in DMSO) at room temperature (RT) for 16−18 h. Modified backbone DNA was purified using PD-10 desalting columns (GE Healthcare) and concentrated in a speed-vacuum. Concentrations were determined using the DNA absorbance $\varepsilon_{260\,nm}$ of 379 051 M^{-1} cm^{-1} on an

Table 1. Photophysical and FRET Properties of the QDs and Fluorophores Used

fluorophores	quantum yield[a]	extinction coefficient (M^{-1} cm^{-1})	λ_{max} absorption	λ_{max} emission	[b]R_0 in Å /$J(\lambda)$ in cm^3 M^{-1} Cy3	Cy5	Cy5.5	Cy7	BOBO-3
530 nm QD	0.20	~1 200 000 (at 300 nm)	–	530 nm	60/6.67e^{-13}	49/1.95e^{-13}	46/1.48e^{-13}	38/4.94e^{-14}	58/5.96e^{-13}
530 nm QD	0.30	~1 200 000 (at 300 nm)	–	530 nm	60/6.14e^{-13}	49/1.93e^{-13}	47/1.48e^{-13}	40/5.40e^{-14}	59/6.15e^{-13}
Cy3	0.14	150 000	550 nm	570 nm	–	53/8.51e^{-13}	51/6.67e^{-13}	45/3.19e^{-13}	54/9.53e^{-13}
Cy5	0.27	250 000	649 nm	670 nm	–	[c]69/2.51e^{-13}	75/3.54e^{-12}	65/1.50e^{-12}	–
Cy5.5	0.28	250 000	675 nm	694 nm	–	–	–	70/2.26e^{-12}	–
Cy7	–	200 000	746 nm	776 nm	–	–	–	–	–
BOBO-3	0.39	147 800	570 nm	602 nm	–	71/1.77e^{-12}	69/1.49e^{-12}	64/9.47e^{-13}	53/3.06e^{-13}

[a] Determined from dye-labeled DNA versus standards. [b] Determined treating each dye as an acceptor to the donor listed in the fluorophore column. For QD donors, accounts for QY increases when assembled with DNA. [c] Cy5 homoFRET R_0 for the configurations in Figure 3D,E. All other homoFRET interactions are negligible.

Agilent Technologies 8453 UV−visible spectrophotometer (Santa Clara, CA). The final peptido−DNA ligate was produced by reacting HYNIC-modified $(His)_6$-peptide (1 mM in 10% DMSO/0.1 M ammonium acetate, NH_4OAc, pH 5.5) with aldehyde-modified DNA (2 mM) in the presence of 100 mM aniline at RT overnight, see Figure 1C. The resulting conjugate was purified using Ni-NTA media (Qiagen, Valencia CA) desalted on an oligonucleotide purification cartridge (Applied Biosystems, Foster City, CA), quantitated using the conjugated hydrazone bond absorption ($\varepsilon_{354\,nm}$ = 29 000 M^{-1} cm^{-1}), dried in a speed-vacuum, and stored at −20 °C until used as detailed in Sapsford et al.[32]

DNA Hybridization and Self-Assembly of Quantum Dot−DNA Photonic Wires. For each configuration described, aliquots of $(His)_6$-peptide-modified backbone DNA stock solution were mixed together with the indicated dye-labeled or unlabeled DNA sp segments in a 500 μL tube (both reconstituted in 1× PBS), placed in a water bath at 100 °C for 5 min, and subsequently allowed to cool to 25 °C ambiently. The ratio of each unlabeled sp or acceptor dye-labeled DNA segment to backbone DNA was always maintained at 1:1 (equimolar amounts). Unlabeled sp segments always replaced dye-labeled segments to maintain the double-stranded DNA structure. Hybridized DNA solutions were mixed with QD stock solutions in 1× PBS for 1 h at RT to yield self-assembled QD−DNA conjugates in 100 μL volumes with final QD concentrations of 0.25 μM.[33] Ratios of 4 peptide−DNA conjugates per QD were used unless indicated. BOBO-3 iodide was purchased from Invitrogen (Carlsbad, CA) and when utilized preincubated with the hybridized peptido−DNA at the indicated concentrations for 1 h in the dark prior to self-assembly to the QDs.

Data Collection and Förster Resonance Energy Transfer Analysis. Steady-state ensemble fluorescence spectra corrected for instrumental effects were collected from solutions of QD−DNA bioconjugates and control QD or DNA-bioconjugates on a Tecan Safire Dual Monochromator Multifunction Microtiter Plate Reader (Tecan, Research Triangle Park, NC) using 300 nm excitation. Pertinent QD/dye photophysical and FRET properties are listed in Table 1. For ET efficiency analysis, the direct excitation contribution to the emission from each acceptor (determined from control solutions) was subtracted from the measured spectra and the resulting composite spectra were deconvoluted to identify the contributions from the QD emission and the sensitized component of each dye in a particular configuration, similar to the methods described previously.[24,34] Note, some data in the figures are presented without deconvolution. For each QD− or dye−dye donor−acceptor pair, the Förster distance R_0 corresponding to a donor−acceptor separation resulting in 50% energy transfer efficiency was calculated using the expression:[17]

$$R_0 = 9.78 \times 10^3[\kappa^2 \breve{n}^{-4} Q_D J(\lambda)]^{1/6} \quad (1)$$

where $\breve{n}$ is the refractive index of the medium, Q_D is the fluorescence quantum yield (QY) of the donor, $J(\lambda)$ is the spectral overlap integral, and κ^2 is the dipole orientation factor. We use a κ^2 of 2/3 which is appropriate for the random dipole orientations found within these self-assembled configurations as detailed previously.[25,35,36] The average energy transfer efficiency E was extracted for each set of QD/dye−dye donor−acceptor conjugates using the expressions:

$$E = \frac{(F_D - F_{DA})}{F_D}, \text{ for steady-state data} \quad (2)$$

or

$$E = \frac{(\tau_D - \tau_{DA})}{\tau_D}, \text{ for time-resolved data} \quad (3)$$

where F_D and F_{DA} are, respectively, the fluorescence intensities of the donor alone and donor in the presence of acceptor(s); similarly, τ_D and τ_{DA} designate the QD excited-state lifetimes of the donor alone and when complexed with the acceptor(s).[17] Within each multifluorophore configuration, the ET for each step is estimated by treating the previous dye as a unique donor and comparing interactions in the presence/absence of the acceptor regardless of how the donor was excited (direct or sensitized). The polyhistidine-driven self-assembly of dye-labeled DNA to QD yields a central nanocrystal conjugated to a centro-symmetric distribution of acceptors characterized by consistent average center-to-center separation distances (r).[25] When analyzed using Förster dipole−dipole formalism, the energy transfer efficiency data can be fit to the expression:[25]

$$E = \frac{nR_0^6}{nR_0^6 + r^6} \quad (4)$$

where n is the average number of acceptors per QD. For conjugates self-assembled with small numbers of acceptors (<4), heterogeneity in conjugate valence can be accounted for by using a Poisson distribution function, $p(N,n)$, during the fitting of the efficiency data:[36]

(31) Prashun, D. E.; Blanco-Canosa, J. B.; Vora, G. J.; Delehanty, J. B.; Susumu, K.; Mei, B. C.; Dawson, P. E.; Medintz, I. L. *ACS Nano* **2010**, *4*, 267–278.
(32) Sapsford, K. E.; Farrell, D.; Sun, S.; Rasooly, A.; Mattoussi, H.; Medintz, I. L. *Sens. Actuators, B* **2009**, *139*, 13–21.
(33) Sapsford, K. E.; Pons, T.; Medintz, I. L.; Higashiya, S.; Brunel, F. M.; Dawson, P. E.; Mattoussi, H. *J. Phys. Chem. C* **2007**, *111*, 11528–11538.
(34) Goldman, E. R.; Clapp, A. R.; Anderson, G. P.; Uyeda, H. T.; Mauro, J. M.; Medintz, I. L.; Mattoussi, H. *Anal. Chem.* **2004**, *76*, 684–688.
(35) Medintz, I. L.; Konnert, J. H.; Clapp, A. R.; Stanish, I.; Twigg, M. E.; Mattoussi, H.; Mauro, J. M.; Deschamps, J. R. *Proc. Natl. Acad. Sci. U.S.A.* **2004**, *101*, 9612–9617.
(36) Pons, T.; Medintz, I. L.; Wang, X.; English, D. S.; Mattoussi, H. *J. Am. Chem. Soc.* **2006**, *128*, 15324–15331.

Table 2. Estimated Donor Energy Losses and Acceptor Sensitized Emission Efficiencies for QDs and Fluorophores in Selected Configurations

Configuration	QD[4]	Cy3	Cy5	Cy5.5	Cy7
Donor / Acceptor positions: 1 2 3 4	**Donor loss**		**Acceptor emission**		
QD[1]	0%				
QD – Cy3	71%	25%			
QD – Cy3 – Cy5	72%	8.8%	5.3%		
QD – Cy3 – Cy5 – Cy5	74%	5.2%	4.8%[3]		
QD – Cy3 – Sp – Sp – Cy5	75%	22%	1.1%		
QD – Cy3 – Sp – Cy5	77%	15%	2.5%		
QD – Cy3 – Cy5 – Sp – Cy5	72%	6.3%	4.5%[3]		
QD – Sp – Cy5 – Cy5	37%	--	2.7%[3]		
Above data from Figure 3D,E.					
QD[2]	0%				
QD – Cy3	75%	18%			
QD – Cy3 – Cy5	88%	7.5%	2.2%		
QD – Cy3 – Cy5 – Cy5.5	84%	6.3%	2.3%	1.0%	
QD – Cy3 – Cy5 – Cy5.5 – Cy7	78%	6.0%	2.0%	0.3%	0%
Donor / Acceptor positions: 1 2 3 4		**Donor loss[5]**	**Acceptor emission**		
Cy3		0%			
Cy3 – Cy5		50%	8.2%		
Cy3 – Cy5 – Cy5.5		49%	2.7%	0.5%	
Cy3 – Cy5 – Cy5.5 – Cy7		50%	2.7%	0.5%	0%
Above 2 data sets from Figure 5B-D.					

530 nm QDs: [1]QY = 0.3 / [2]QY = 0.2. [3]Multiple Cy5 acceptors treated as a single dye. [4]QD donor-loss when interacting with 4-acceptors/QD. [5]Cy3 donor interacting with 1 acceptor. QD/dye-donor emission values derived from PL loss using deconvoluted emission profiles. Acceptor sensitized emission/end-to-end efficiencies are highlighted in red and are normalized to one DNA strand per QD and estimated using eq 8 while treating each indicated dye as the terminal acceptor. Values >10% rounded up.

$$E = \sum_n p(N,n)E(n) \quad \text{and} \quad p(N,n) = N^n \frac{e^{-N}}{n!} \tag{5}$$

where n designates the exact numbers of acceptors (valence) for conjugates with a nominal average valence of N.

Fluorescence lifetime measurements were performed using a time-correlated single-photon counting (TCSPC) system with a temporal resolution of 50 ps as described in the Supporting Information.[37] Fluorescence intensities were integrated over narrow windows centered at 530 nm for the QD, 625 nm for Cy3, and 680 nm for Cy5 dye. The latter emission windows were positioned at wavelengths longer than their respective dye-emission maxima to minimize signal cross-talk from either QD or QD-Cy3 emissions, respectively. Fluorescence decay traces of the QD signal with time (collected for the indicated dye-to-QD ratio, n) were fit to a two or three-exponential function:

$$I(t) = A_1 e^{-t/\tau_1} + A_2 e^{-t/\tau_2} + A_3 e^{-t/\tau_3}, \tag{6}$$

where t is time, and A_i is weighting parameter associated with each decay time. An average amplitude-weighted lifetime defined as:

$$\tau_D = (A_1\tau_1 + A_2\tau_2 + A_3\tau_3)/(A_1 + A_2 + A_3) \tag{7}$$

was extracted from the fit using FluoFit (Picoquant, Berlin Germany). For samples showing a significant initial rise time component, a reconvolution procedure incorporating the instrument response was utilized to analyze the pertinent decay and rise time data.

Sensitized acceptor emission and end-to-end energy transfer efficiencies within select configurations were estimated using the methodology outlined by Hannestad,[5] see Table 2. Briefly, the number of sensitized dye-acceptor molecules is compared to the number of initially excited QD- or dye-donor molecules while also accounting for QYs. This analysis is applied to both the terminal acceptors and for intermediary acceptors by treating them as the terminal acceptor following deconvolution and correction of the direct excitation component. After dividing the extracted terminal dye-emission by its fluorescence QY (Table 1), a measure of the total excitation energy transferred by the donor through the system to an acceptor is derived. Similarly, the initial QD or dye emission is adjusted by its QY to estimate the number of initially excited donor molecules. This is described by:[5]

$$E = \frac{(F_{AD} - F_A)/Q_A}{F_D/Q_D} \tag{8}$$

where F_{AD} and F_A are the integrated acceptor emission spectra on the wavenumber scale using 300 nm excitation in the presence and absence of donor, respectively. F_D is the integrated donor emission from a corresponding configuration containing only that donor. Q_D and Q_A are the QY's of the donor and acceptor, respectively. This value is distinct from FRET efficiency described above. That describes loss of donor PL in the presence of acceptor, while this incorporates sensitized acceptor emission in the overall estimate of energy transfer efficiency and provides insight into other acceptor decay channels along with acceptor QY following sensitization.

Results and Discussion

DNA Sequences, His_6-Peptide Modification, and Metal-Affinity Coordination to QDs. Figure 1 provides an overview of the conjugation strategy used to assemble the QD−photonic wires along with the DNA sequences, their respective dye labels, the peptide sequence, and the chemoselective ligation chemistry utilized. The specific dsDNA sequence utilized is based on Ouchi's work and incorporates several important structural criteria including: (1) the final ds-structure is rigid and does not assume other 3-dimensional structures arising from intramolecular H-bonding, (2) the chromophore labeling sites are located every 10 residues (~33 Å) placing them all on the same side of the DNA-duplex and separating them by one helical turn, and (3) A−T pairs are specifically located near the chromophores to avoid guanine-induced quenching.[10] This placement does not, however, account for the 3-carbon linkers which attach the dye to the DNA terminus nor for the dye structure itself,

(37) Medintz, I. L.; Pons, T.; Susumu, K.; Boeneman, K.; Dennis, A.; Farrell, D.; Deschamps, J. R.; Melinger, J. S.; Bao, G.; Mattoussi, H. *J. Phys. Chem. C* **2009**, *131*, 18552–18561.

both of which combine to allow the dyes some freedom of rotational movement. The 'backbone' or template strand was obtained as a contiguous 40-mer with a free primary amine attached to the 3′ end via a 7-carbon alkane linker. Sequential 10-bp DNA segments designated 1−4, respectively, and complementary to the backbone strand were obtained as either unlabeled sp (spacer) segments or labeled with the indicated acceptor dyes at their 5′ end (Figure 1B). An alternate segment 4 was obtained with an amine-modified T which was subsequently labeled with Cy7 dye. The design provides for a final hybridized structure where oligos 1−4 and their dyes will be sequentially arranged on the same side of the dsDNA and separated from each other by one helical turn.

To facilitate DNA attachment to QDs, we utilize a self-assembly approach based on polyhistidine $(His)_n$-driven metal-affinity coordination. This interaction occurs between the imidazolium side chain groups on oligohistidine-sequences and the Zn-rich surface of CdSe/ZnS core/shell QDs.[33] We, and others, have demonstrated that various types of QD preparations can be self-assembled with proteins, peptides, and modified DNA expressing clearly available $(His)_n$-sequences in a rapid manner (<30 min) due to the high affinity equilibrium binding constants of this interaction ($K_{eq} \sim 1 \times 10^9$ M^{-1}).[31,33,38−45] Control can be exercised over both the ratio or valence of molecules self-assembled per QD through the molar equivalents used and even allows for spatial orientation of biomolecules on the QD surface in most cases.[35−37] For the current purposes, we exploit aniline-catalyzed hydrazone ligation chemistry to join the modified backbone DNA to a $(His)_6$-peptidyl sequence. This chemistry, originating from the Dawson lab, is characterized by enhanced bioconjugation rates of 10^1-10^3 M^{-1} s^{-1} in mild, aqueous conditions (slightly acidic to neutral pH) and goes to completion within 30 min using 100 mM aniline with 10 μM of reactants.[30,46] As the hydrazine and aldehyde reactive groups are orthogonal to most common biological functionalities, they do not alter the subsequent structure or capabilities of the $(His)_6$-peptide or DNA. The primary amine on the backbone DNA was modified to an aldehyde and then chemoselectively ligated to the HYNIC-modified $(His)_6$-peptide sequence as detailed in the Materials and Methods. Individual dye-labeled DNA strands were then hybridized to their complementary sequence on the $(His)_6$-modified DNA backbone and ratiometrically self-assembled to the QDs to yield the final QD−DNA photonic wire nanostructure. The ability of $(His)_6$−peptido−DNA constructs to ratiometrically self-assemble to QDs has been repeatedly confirmed.[31,41,42,45]

Spectral Overlap of the Quantum Dot and Dye Fluorophores. Figure 2 presents the superimposed absorption and emission spectra of the QD and dye-fluorophores utilized in this study. Table 1 lists the relevant photophysical parameters including the Förster distances or R_0 values along with the spectral overlap integrals $J(\lambda)$. These were derived by treating the QD or each individual fluorophore as a single donor interacting with each increasingly red-shifted fluorophore as acceptor.[17] As plotted in Figure 2A, beginning with the 530 nm QD and extending to the Cy7 absorption, a pattern of consecutive absorption/emission profiles is clearly evident; there are contiguous spectral overlap(s) from the QD emission to the Cy7 absorption. Only the Cy7 absorption is shown here as no fluorescence emission was observed for this dye (vide infra). The absorption of the BOBO-3 DNA intercalating dye overlaps with that of the 530 nm QD and Cy3 dye, while the broad emission extends through the Cy5, Cy5.5, and Cy7 absorption profiles, Figure 2B. Depending on the degree of spectral overlap and the acceptor extinction coefficient, the R_0 values range from 38 Å for the 530 nm QD−Cy7 pair to 75 Å for Cy5 donor interactions with Cy5.5. BOBO-3 interactions with Cy5 and Cy5.5 are nearly equivalent (71 and 69 Å, respectively) due to the slightly broader Cy5.5 absorption spectrum. We also note that the R_0 value for both 530 nm QD samples with Cy3 acceptor are the same (60 Å) despite the difference in QY (0.20 vs 0.30), as the first QD sample has a slightly broader emission spectrum. The repeated ∼33 Å periodicity of dye-attachment points across the final 132 Å dsDNA structure in conjunction with the R_0 values (all significantly larger than 33 Å) suggest that multiple, consecutive FRET interactions or a vectorial FRET cascade should occur with relatively high efficiency between the fluorophores when appropriately arranged on the DNA.

Configuration 1: 530 nm QD-Cy3-Cy5. The first QD−photonic wire construct consisted of 530 nm QDs (QY = 0.3) self-assembled with the $(His)_6$-modified DNA displaying Cy3 and Cy5 dyes. The latter Cy5 dyes were alternated among several positions along the wire, see Figure 3A for a schematic. Initial experiments focused on evaluating FRET efficiency E between the central QD and a Cy3 dye-acceptor labeled on DNA segment 1 (closest to the QD) as the ratio of conjugated Cy3-labeled-DNA was incrementally increased from 0.5 to 8 per QD. The $(His)_6$-modified backbone DNA was prehybridized with equimolar 1:1 concentrations of Cy3-labeled segment 1 and unlabeled segments 2−4 and then self-assembled to the 530 nm QDs as described in Materials and Methods. Figure 3B shows representative direct-acceptor excitation corrected and deconvoluted PL spectra collected from both the QD donors and Cy3 dye acceptors as the discrete donor/acceptor (QD/DNA) ratios were varied. Figure 3C plots the resulting FRET E calculated using eq 2, the FRET E corrected for assembly heterogeneity using the Poisson distribution function in eq 5 along with Cy3 sensitization.[36] As expected, data show a clear loss in QD donor PL and a corresponding increase in sensitized Cy3 acceptor emission which directly tracks the increasing number of acceptors $(peptide-DNA)_n$ arrayed around the central QD nanoscaffold.

The average QD-Cy3/donor−acceptor center-to-center separation distance r calculated from this data yielded a nominal value of ∼73 Å. A predicted separation distance can be derived by considering the pertinent variables including: (i) A 530 nm emitting CdSe core QD with around ∼4 to 5 monolayers of ZnS overcoating can be expected to have a hard radius of ∼27−29 Å.[26] (ii) For the peptide portion, 4−5 of the $(His)_6$

(38) Dennis, A. M.; Bao, G. *Nano Lett.* **2008**, *8*, 1439–1445.
(39) Dif, A.; Henry, E.; Artzner, F.; Baudy-Floc'h, M.; Schmutz, M.; Dahan, M.; Marchi-Artzner, V. *J. Am. Chem. Soc.* **2008**, *130*, 8289–8296.
(40) Liu, W.; Howarth, M.; Greytak, A. B.; Zheng, Y.; Nocera, D. G.; Ting, A. Y.; Bawendi, M. G. *J. Am. Chem. Soc.* **2008**, *130*, 1274–84.
(41) Medintz, I. L.; Berti, L.; Pons, T.; Grimes, A. F.; English, D. S.; Alessandrini, A.; Facci, P.; Mattoussi, H. *Nano Lett.* **2007**, *7*, 1741–1748.
(42) Berti, L.; D'Agostino, P. S.; Boeneman, K.; Medintz, I. L. *Nano Res.* **2009**, *2*, 121–129.
(43) Boeneman, K.; Delehanty, J. B.; Susumu, K.; Stewart, M. H.; Medintz, I. L. *J. Am. Chem. Soc.* **2010**, *132*, 5975–5977.
(44) Blanco-Canosa, J. B.; Medintz, I. L.; Farrell, D.; Mattoussi, H.; Dawson, P. E. *J. Am. Chem. Soc.* **2010**, *132*, 10027–10033.
(45) Yeh, H. Y.; Yates, M. V.; Mulchandania, A.; Chen, W. *Chem. Commun.* **2010**, *46*, 3914–3916.
(46) Dirksen, A.; Hackeng, T. M.; Dawson, P. E. *Angew. Chem., Int. Ed.* **2006**, *118*, 7743–7746.

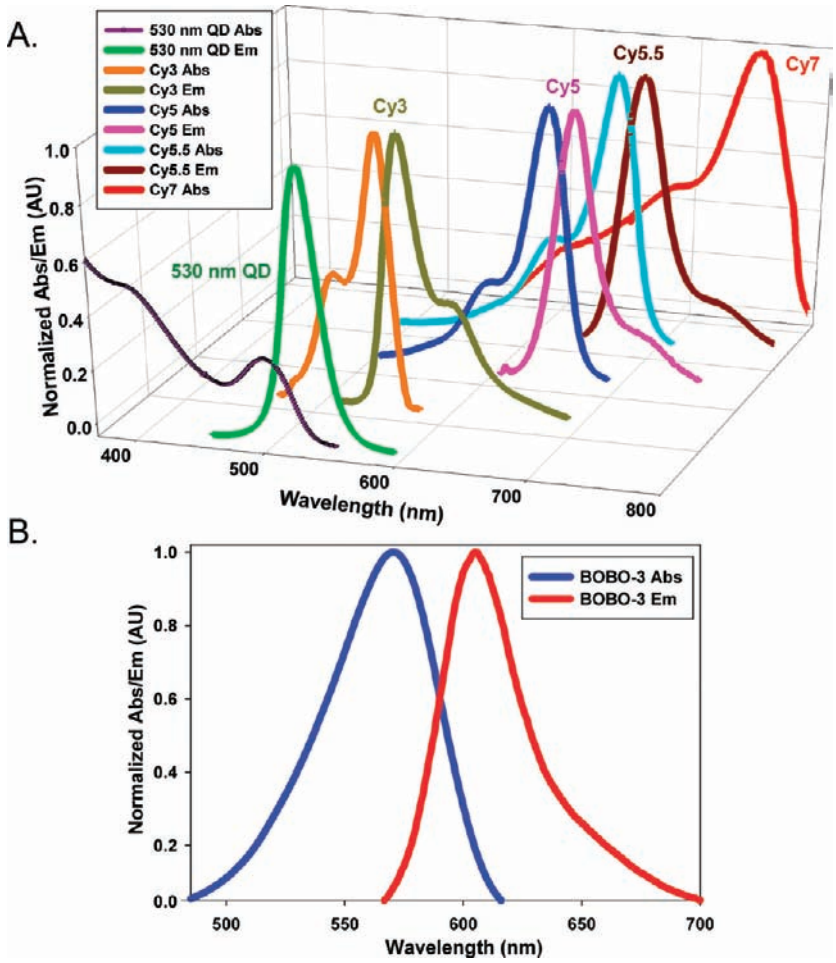

Figure 2. Spectral overlap. Three-dimensional plot showing the absorption and emission of the 530 nm emitting QD along with that of the Cy3, Cy5, Cy5.5, Cy7, and BOBO-3 dyes utilized. As Cy7 dye emission was not observed, it is not included.

residues can be ignored as they are predicted to be directly attached to the QD surface leaving a predicted extension of ≤15 Å for the rest of this peptidyl sequence.[47] (iii) The hydrazone chromophore will have a length of ≤5 Å. (iv) The DNA backbone is linked to the bisarylhydrazone by a 7-carbon alkane linker of ∼8 Å length. (v) The Cy3 is attached to the 5′ end of DNA segment 1 by a 3-carbon linker and a phosphate bond with a combined ∼7−10 Å length. (vi) Lastly, Cy3 itself is a relatively linear molecule with a fully extended conformation of <10 Å, see Supporting Information for pertinent structures. Comparison to the empirically derived 73 Å separation distance shows an excellent agreement to the ∼77 Å maximum expected when summing these values. This result suggests that the DNA structure is attached to the QD surface and extending directly out in a linear manner and is not folding back either on itself or over the QD surface consistent with previous results attaching DNA to QDs in a similar manner.[41,42] More importantly, acceptors placed at different points on the DNA will extend away and be centro-symmetrically arranged at fixed distances in relation to the QD core. We attribute the rigidity of the QD−DNA extended structure in part to steric effects from the PEGylated ligands used to make the QDs hydrophilic. The ∼15 ethylene oxide repeats found within the DHLA−PEG ligand structure should allow the PEG portion to extend at least 25−35 Å away from the QD surface in an energy minimized conformation (data not shown) while their density prevents the DNA from folding back across the nanocrystal surface.

As the focus was to investigate energy transfer from central QDs to surrounding DNA photonic wires, we used Figure 3B,C to select an optimal acceptor ratio or (peptide−DNA)$_n$/QD of 4 for use in experiments as this assures a more consistent acceptor/donor ratio as dictated by Poissionian statistics.[36,48] This relatively low valence also ensures minimal acceptor interactions or 'cross-talk' and homoFRET between dyes on the DNA strands when attached to QDs. Use of a constant (His)$_6$−DNA ratio also minimizes fluctuations from any QD PL increases which are believed to arise from improved surface passivation following conjugation.[25] For example, a ∼20% PL increase in QD PL from conjugation to 4-unlabeled peptide−DNAs can be seen in Figure 3D (vide infra) and is accounted for in determining efficiencies. Note, data presented in all subsequent experiments utilize a central QD assembled with 4 (His)$_6$−DNAs while the number, type, and position of acceptor dyes on the DNA are modified unless otherwise stated; spectra reflect interactions of a single QD with 4 of each indicated acceptor.

Subsequent experiments monitored ET efficiency in the same configuration described in Figure 3A−C while the number of linearly arranged acceptors extending out from the QD was

(47) Medintz, I. L.; Sapsford, K. E.; Clapp, A. R.; Pons, T.; Higashiya, S.; Welch, J. T.; Mattoussi, H. *J. Phys. Chem. B.* **2006**, *110*, 10683–10690.

(48) Pons, T.; Uyeda, H. T.; Medintz, I. L.; Mattoussi, H. *J. Phys. Chem. B.* **2006**, *110*, 20308–20316.

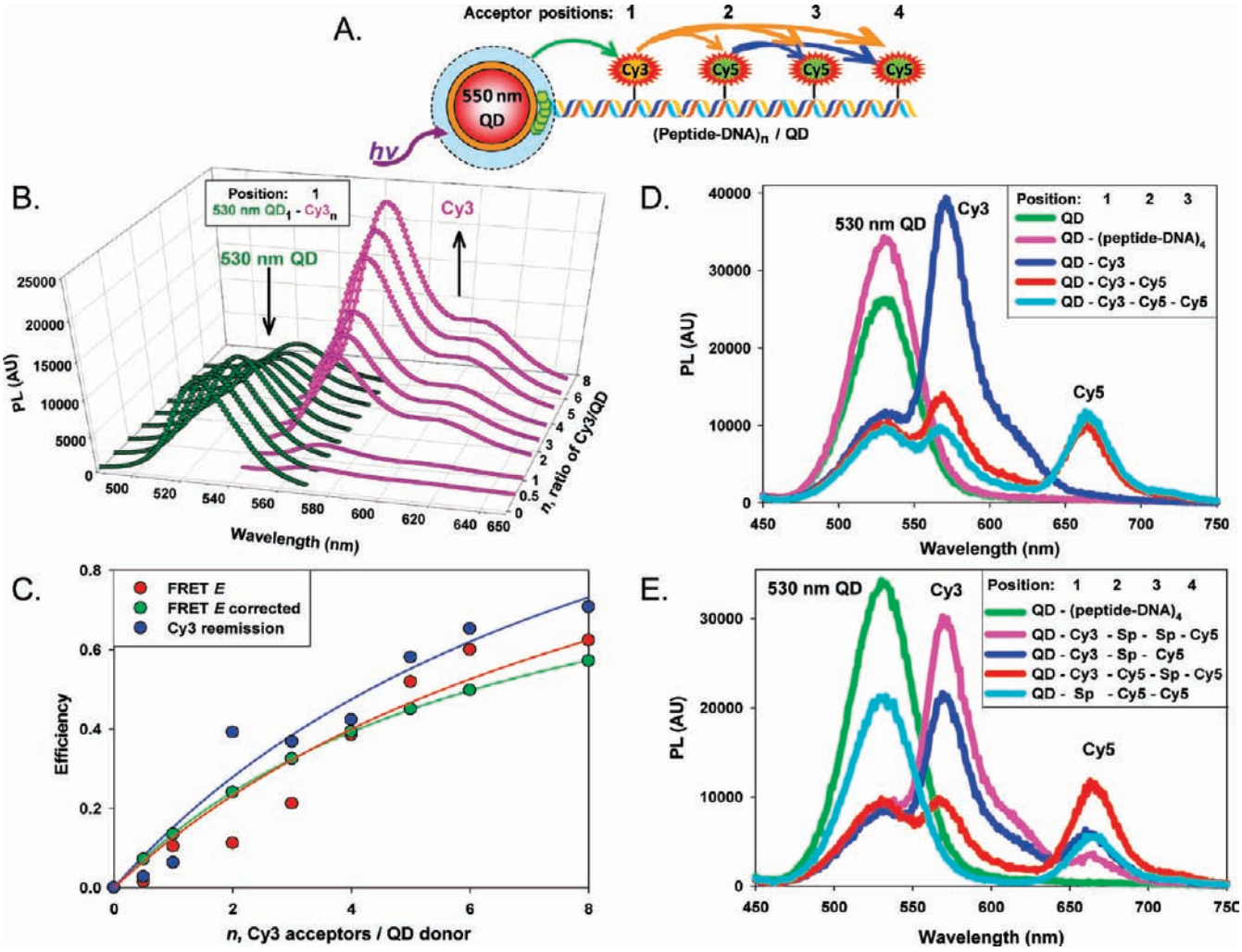

Figure 3. Configuration 1: 530 nm QD-Cy3-Cy5. (A) Schematic of the configuration consisting of 530 nm QDs self-assembled with an increasing ratio of $(His)_6$−peptide−DNA hybridized with Cy3 in position-1 and single or multiple Cy5-labeled DNA in positions-2−4. (B) Deconvoluted PL spectra from 530 nm QD donors self-assembled with an increasing ratio of $(His)_6$−peptide−DNA with Cy3 acceptor located in position-1. (C) Plots of FRET efficiency *E*, FRET *E* corrected determined using eq 4, and Cy3 sensitized emission. (D) Composite PL spectra from 530 nm QD donors, 530 nm QD donors self-assembled with unlabeled DNA, DNA with Cy3 in position-1, Cy3 in 1/Cy5 in 2, and Cy3 in 1/Cy5 in 2,3. (E) Composite PL spectra from 530 nm QD donors self-assembled as in panel D with unlabeled DNA and unlabeled spacer 'sp' SEGMENTS REPLACING CY3 IN POSITION-1 and Cy5 in positions-2−4 as indicated. A ratio of 4 dye-labeled $(His)_6$−peptide−DNA/QD used for all configurations shown in panels D and E. Representative spectra are shown in the images; however, each configuration was assembled and tested at least 4−6 times to confirm the results.

increased to include a Cy5 dye in position-2 and/or 3. Figure 3D confirms that as Cy3 acceptor is placed in position-1, a substantial sensitization of the 4 surrounding Cy3 acceptors is noted with a corresponding loss of central QD donor PL. The normalized end-to-end energy transfer efficiencies estimated using eq 8 show that only 25% of the initial QD excitation energy available is being subsequently emitted by the Cy3 dyes, see efficiencies in Table 2. This shows that, although the Cy3 acceptor is clearly an effective quencher in this role, the sensitization that it could provide to the next acceptor may be decreased due to the presence of other competing nonradiative decay pathways. Replacing the unlabeled DNA spacer in position-2 with a Cy5-labeled segment significantly quenches the Cy3 as it is now sensitizing this proximal acceptor. In this configuration, we see that QD PL loss remains essentially unchanged; however, the intermediary Cy3 dyes are now >60% quenched and the terminal Cy5 emits ∼5% of the original excitation energy going into the system. An extension to this system placed a second Cy5 dye acceptor in position-3. Although this added Cy5 dye is further removed from the QD/Cy3 positions, it should still draw energy from the Cy3 while also engaging in homoFRET with the intermediary Cy5 due to both excellent spectral overlap (R_0 ∼69 Å) and close proximity. This should optimize ET from the QD through Cy3 system to the Cy5 acceptors in positions-2,3. In agreement with this, the data show a further 20% drop in Cy3 emission and a small increase in overall Cy5 sensitization although the estimate of end-to-end efficiency was essentially unchanged when normalized.

Cognizant of the fact that multiple interactions will occur among all participants in such extended conformations with efficiencies that are dictated by both separation distance and the degree of spectral overlap present, we estimated some of the longer-range ET contributions in this structure by either moving the acceptors to different positions or replacing selected Cy3/Cy5 dyes with unlabeled spacers (sp), see Figure 3E and Table 2. Moving the terminal Cy5 from position-3 to 4 in the 2-Cy5 acceptor system described above results in overall ET efficiency through the system (QD-Cy3-Cy5-sp-Cy5) that is not significantly different. This was expected as the Cy5 acceptor in position-2 is expected to be dominant. By then removing the

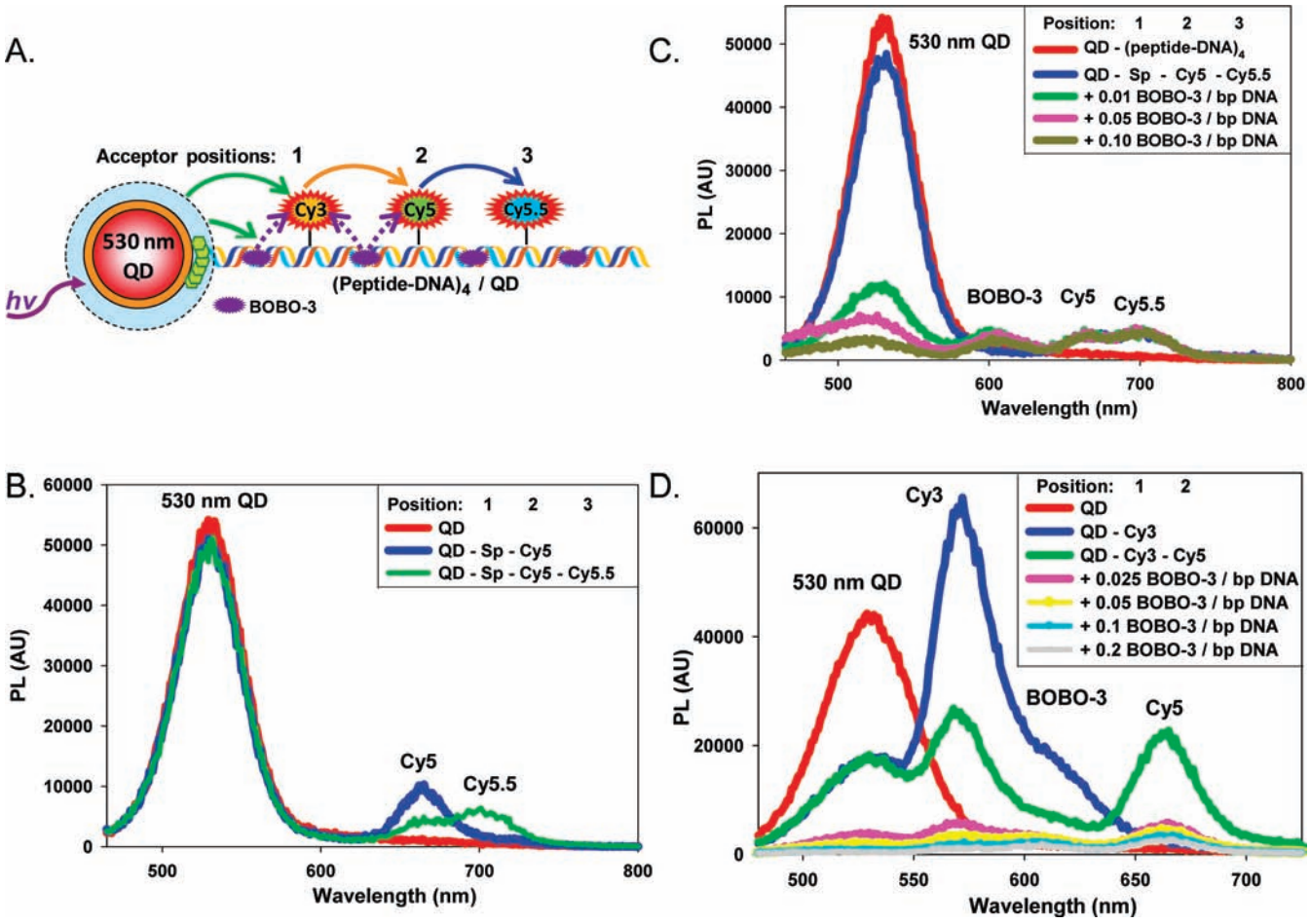

Figure 4. Configuration 2: 530 nm QD-Cy3-Cy5-Cy5.5 with BOBO-3 intercalating dye. (A) Schematic of the configuration consisting of 530 nm QDs self-assembled with 4 $(His)_6$−peptide−DNA hybridized with Cy3 in 1/Cy5 in 2/Cy5.5 in 3 and BOBO-3 dye intercalated into the DNA. (B) Composite PL spectra from 530 nm QD donors self-assembled with unlabeled sp segments in 1/Cy5 in 2/Cy5.5 in 3. (C) Composite PL spectra from 530 nm QD donors self-assembled as in panel B with unlabeled DNA and with the indicated ratios of BOBO-3 per bp DNA. (D) Composite PL spectra from 530 nm QD donors self-assembled with unlabeled DNA, DNA with Cy3 in position-1, Cy3 in 1/Cy5 in 2, and with the indicated ratios of BOBO-3 per bp DNA.

intermediary Cy5 in position-2 (QD-Cy3-sp-Cy5), we verify this dominant role as the Cy3 recovers from ∼5% to 15% overall emission efficiency even though it is still partially quenched due to the remaining interactions with the distal Cy5 in position-3. Moving the Cy5 to position-4 and placing 2 unlabeled spacers in positions-2,3 (QD-Cy3-sp-sp-Cy5) allows the Cy3 emission an almost full recovery while only ∼1% of the excitation energy is emitted by the terminal Cy5 dye. Similarly, removing the Cy3 dye in position-2 while leaving Cy5 dyes in positions-2,3 (QD-sp-Cy5-Cy5) significantly drops the rate of FRET quenching observed for the central QD to 37% from ∼74% while Cy5 emission efficiency is only ∼3%. These controls confirm that, although such longer range ET interactions do occur, transfer to more proximal acceptors with better spectral overlap clearly dominates in these linear arrangements.

Configuration 2: 530 nm QD-Cy3-Cy5-Cy5.5 with BOBO-3 Intercalating Dye. An alternate series of QD-wires, where the dsDNA scaffold itself was also labeled with an intercalating dye, were next investigated. This family of functionally analogous dyes is characterized by a high propensity to engage in homoFRET interactions, which, in this context can allow energy to be conveyed in a diffusive manner without concomitant losses from the downhill transfer associated with increasingly red-shifted emissions.[5,17] The exact placement of intercalating dye in a DNA structure cannot be controlled; however, combining optimal spectral overlap with judicious choice in the ratio of dye used for labeling should allows efficient ET by providing multiple dyes with similar average spacing's and hence interactions spread across the DNA span.[5] In this case, the dimeric cyanine intercalator BOBO-3 iodide was utilized as it provides excellent spectral overlap with the 530 nm QDs and Cy3 dye donors (R_0 of 59 and 54 Å, respectively, as acceptor) and Cy5, Cy5.5, Cy7 when acting as the donor itself while also displaying a relatively strong quantum yield of 0.39, see Figure 2 and Table 1. Figure 4A shows a schematic overview of the two different configurations tested with this dye.

The first configuration replaced the Cy3 dye with an unlabeled spacer at position-1 and placed Cy5 and Cy5.5 as distal acceptors at positions-2 and 3, respectively. Figure 4B shows representative composite spectra from the 530 nm QDs self-assembled with 4-unlabeled peptido−DNAs, with Cy5 in position-2, and Cy5/Cy5.5 in positions-2/3. Although the QDs utilized in these structures have a QY of ∼0.3, very little FRET quenching of the QD is seen in the presence of either Cy5 alone or both acceptors. Comparing these results to those described in Figure 3 above confirms a much lower rate of Cy5 FRET sensitization and examining the corresponding Cy5-labeled DNA-only controls suggested that >90% of the observed Cy5 emission here results from direct excitation (data not shown). Placement of Cy5.5 in position-3 significantly quenches the Cy5

fluorescence by >50% without any change in the QD PL confirming that this added acceptor draws energy predominantly from the much closer Cy5 donor. Clearly, the lack of Cy3 as an intermediary or relay in this QD-wire structure leaves the central QD donor significantly unquenched while Cy5 and Cy5.5 together receive very little direct sensitization. Figure 4C shows data where addition of BOBO-3 dye to the wires was tested at average ratios of 0.01, 0.05, and 0.10 dye-per bp total dsDNA. These labeling ratios correspond to an average of ~1 dye molecule per 100, 50, and 10 bp's of dsDNA present. Thus 1.6, 3.2, and 16 BOBO-3 dyes on average can be expected within the dsDNA surrounding each QD donor, respectively. For the latter 2 values, this should place most BOBO-3 dyes within sufficient distance of one another to allow for significant homoFRET (R_0 ~53 Å). Even at the lowest ratio, a significant quenching of ~80% of the QD PL is observed and this increases to >95% quenching at the highest intercalator concentration. A small BOBO-3 emission is observed at ~600 nm which also drops with increasing intercalator ratio. No concurrent FRET sensitization or any other changes were seen in the Cy5 and Cy5.5 emissions. This suggests that, although BOBO-3 is a very effective FRET acceptor of QD PL even at low valence, it does not emit or sensitize the distal red dyes efficiently in this configuration. Given these results, we subsequently tested whether BOBO-3 could augment the function of the Cy3 intermediary rather than replace it in the same structure. Figure 4D shows representative data collected from 530 nm QDs self-assembled with an increasing evolution of acceptor dyes that ultimately result in Cy3/Cy5 in position-1/2. These were then assembled in the same manner except for prelabeling the DNA with the indicated ratios of BOBO-3. These ratios translate to ~4, 8, 16, and 32 dyes on average intercalated within the dsDNA surrounding each QD donor, respectively. A similar effect as before was noted here where the higher ratios of BOBO-3 utilized quenched both the QD and Cy3 emission to almost 100%. A 70 to >90% drop in Cy5 emission is observed concomitant with these changes, which is attributed to an almost complete loss in direct sensitization from the QD and Cy3 dye donors. Control experiments with just QDs and BOBO-3 demonstrated minimal interactions/quenching while QD-unlabeled dsDNA assemblies showed similar and significant QD donor quenching (data not shown). Excellent spectral overlap and high BOBO-3 QY suggested placement into the QD DNA wire should have improved coupling and FRET efficiency; however, overall results consistently demonstrate strong quenching. We speculate that much of the quenching is due to BOBO-3 forming nonemissive complexes within the DNA or with the cyanine dyes which may act as energy sinks along with some other possible quenching mechanisms. A detailed discussion of some of the putative reasons behind this can be found in the Supporting Information.

Configuration 3: 530 nm QD-Cy3-Cy5-Cy5.5-Cy7. The third photonic wire construct consisted of 530 nm QDs (QY = 0.2) self-assembled with the $(His)_6$−DNA scaffold where the number of linearly arranged acceptors extending out from the central nanocrystal was sequentially increased to 4 with the addition of Cy3, Cy5, Cy5.5, and last Cy7 dyes in positions-1 through 4, respectively, see Figure 5A schematic. Figure 5B presents the evolution of composite spectra as each increasingly red-shifted acceptor dye is linearly added to the structure and interrogated. As before, the addition of Cy3 in position-1 substantially quenches the central QD and this, in turn, is significantly quenched by the addition of Cy5 in position-2. Cy5 is then quenched by the addition of a Cy5.5 dye in position-3. In contrast to the data in Figure 4B, where Cy5 and Cy5.5 were present in the same terminal positions without an intermediary Cy3 in position-1, the emissions of Cy5 and Cy5.5 are far more pronounced due to increased sensitization through the wire and are ~3× the magnitude of the same directly excited control dyes alone (data not shown). Although the initial QD quenching efficiency is quite high at 80−90% in this configuration, the estimated amount of energy being emitted by the Cy5 and Cy5.5 terminal acceptors is only ~2.2% and 1%, respectively (Table 2). The lower QD QY in combination with the additional ET steps most likely contributes to these modest overall efficiencies. A Cy7-labeled acceptor was then assembled into position-4 to create the final 4-dye QD photonic wire, see Figure 5B for composite spectra and Figure 5C for individual deconvoluted spectra of each component. Although the amount of excitation energy being transmitted through the system and emitted by Cy5.5 is a low 1%, this is still visibly quenched by more than half to ~0.3% by the terminal Cy7 dye. We note no sensitized emission or even directly excited emission from the DNA-labeled Cy7 dye indicating that it functions solely as a near IR quencher in this configuration similar to previous reports.[49]

We next compared this extended central QD/4-surrounding fluorophore wire to those of just the DNA wire itself. Figure 5D shows composite spectral data collected from the same concentrations of DNA wire with no QD present as each increasingly red-shifted acceptor dye is placed into the structure. Although Cy3 does absorb at 300 nm, its extinction coefficient here is ~10% of that at its maxima; thus, to efficiently excite the initial Cy3 donor in position-1 without leakage into other spectral windows, 535 nm illumination was used which is close to the Cy3 absorption maxima of ~555 nm. A 50% loss in Cy3 emission is observed when Cy5 acceptor is placed into position-2 of the structure. This loss in Cy3 emission is smaller in overall magnitude as compared to the same Cy5 addition when the wire is anchored to the central QD. However, the Cy5 emission of 8.2% is ~4× higher than the 2.2% Cy5 emission observed for the same configuration when attached to the QD, see Table 2. This increase may be partially ascribed to the fewer number of ET steps (2 vs 1, in the presence or absence of QD, respectively) between the directly excited donor and the Cy5 acceptor along with some direct excitation. The further addition of Cy5.5 in position-3 quenches the Cy5 >50% while not visibly affecting the Cy3 PL, similar to the results observed for the analogous QD configuration above. Although the Cy3 and Cy5.5 dyes share good spectral overlap with an R_0 of 51 Å and are located within 66−70 Å of each other, which predicts a modest (~5−10%) level of ET, no changes in Cy3 emission are observed. This indicates that Cy5.5 engages almost exclusively in ET with the intermediary Cy5 in both configurations while not drawing from the further Cy3 dye. The Cy5.5 emission efficiency estimated at 0.5% is rather poor in this structure and comparison to individual dye-only controls confirms that almost all of it is attributable to a low direct excitation process (data not shown). Placing a Cy7-labeled acceptor into position-4 to create the final 4-dye DNA-only photonic wire did not alter the Cy5.5 emission visibly regardless of its direct excitation in this configuration.

Directly comparing the two systems above (DNA 4-surrounding fluorophore wire on/off the central QD) indicated that the

(49) Gruber, H. J.; Hahn, C. D.; Kada, G.; Riener, C. K.; Harms, G. S.; Ahrer, W.; Dax, T. G.; Knaus, H. G. *Bioconjugate Chem.* **2000**, *11*, 696–704.

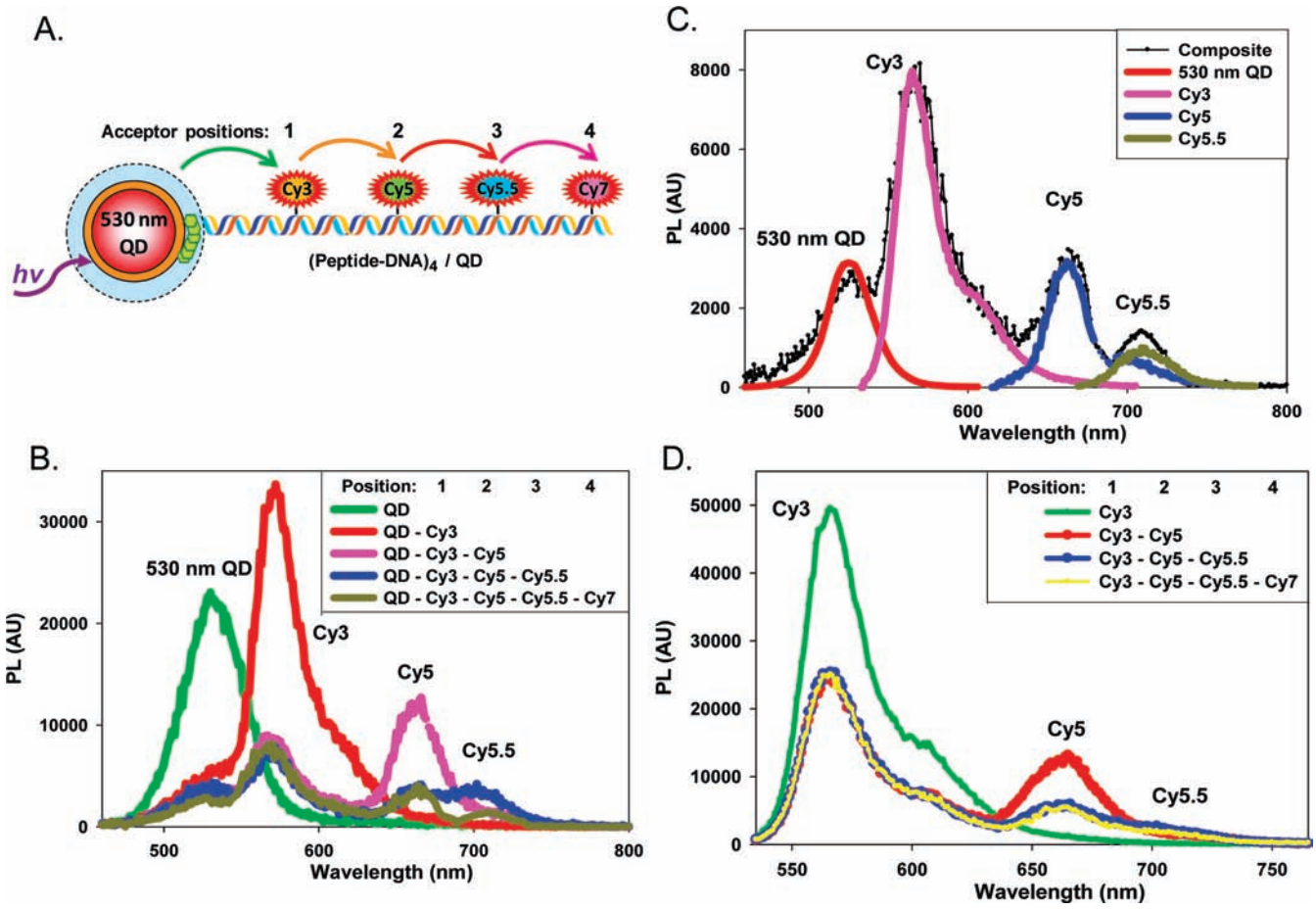

Figure 5. Configuration 3: 530 nm QD-Cy3-Cy5-Cy5.5-Cy7. (A) Schematic of the configuration consisting of 530 nm QDs self-assembled with 4 $(His)_6$−peptide−DNA hybridized with Cy3 in 1/Cy5 in 2/Cy5.5 in 3/Cy7 in 4. (B) Composite PL spectra from 530 nm QD donors self-assembled with unlabeled DNA, DNA with Cy3 in position-1, Cy3 in 1/Cy5 in 2, Cy3 in 1/Cy5 in 2/Cy5.5 in 3, Cy3 in 1/Cy5 in 2/Cy5.5 in 3/Cy7 in 4. (C) Composite PL spectra B with all 4 dye-acceptors along with their deconvoluted individual contributions. (D) Composite spectra from Cy3 in 1, Cy3 in 1/Cy5 in 2, Cy3 in 1/Cy5 in 2/Cy5.5 in 3, Cy3 in 1/Cy5 in 2/Cy5.5 in 3/Cy7 in 4 (no QD present, DNA only). Sample D excited at 535 nm.

central QD donor was capable of augmenting the energy flow through the system. The QD construct was excited at 300 nm where the QD extinction coefficient is $\sim 1.2 \times 10^6$ M^{-1} cm^{-1} while the dye-only construct was excited at 535 nm where its absorption is $\sim 5.1 \times 10^4$ M^{-1} cm^{-1}, over an order of magnitude less. We surmise that these factors, in conjunction with QD excitation at a higher energy portion of the spectrum, all contribute to the better energy flow and may also account for each QD's ability to sensitize 4-proximal DNA photonic structures. This clearly suggests that incorporating QDs into photonic wires imparts improved energy harvesting and sensitization characteristics to these types of assemblies.

Time-Resolved Fluorescence Data. We analyzed the excited-state fluorescence lifetimes of selected configurations to confirm the sequential ET steps involved. QD−DNA wires were assembled as before, and as consecutive acceptors were added, the PL lifetime properties of selected QD/fluorophores were interrogated and compared to controls consisting of the same fluorophore alone in solution, see schematic in Figure 6A. The fluorescence decay signals from the 530 nm QD when assembled with either unlabeled DNA or Cy3 hybridized in position 1 are plotted in Figure 6B. The average QD lifetime (τ_{AV}) was significantly quenched from 14.4 to 5.04 ns (∼65%) by the presence of the 4 proximal Cy3 acceptors. These changes are comparable to the ∼66% changes noted in an analogous 530 nm emitting QD when self-assembled with 5 Cy3-labeled maltose binding proteins (MBP).[25] For that configuration, the labeling site targeted on the protein placed the dye at a slightly longer separation distance from the QD within the conjugate. We next measured fluorescence decay signals from Cy3 at position 1 in the QD−DNA wire as shown in Figure 6C. The 1.33 ns average fluorescence lifetime from control Cy3-labeled DNA increased ∼3.5 times to 4.70 ns when acting as an acceptor for the central QD. This increase reflects the strong QD sensitization in this configuration and is analogous to the increases in Cy3 acceptor sensitized lifetime noted in the previously mentioned QD-labeled MBP configuration.[25] Placing a Cy5 acceptor in position 2 quenches the sensitized Cy3 fluorescence by ∼18% to a τ_{AV} of 3.84 ns confirming that its sensitized emission can in turn be significantly quenched by the addition of a proximal acceptor. Examining the properties of Cy5 in position 2 shows that its native-unbound fluorescence lifetime of 1.33 ns increases ∼3 times to 4.08 ns when sensitized by the Cy3 donor, see Figure 6C. Placement of Cy5.5 in position 3 on the QD−DNA nanowire results in a 30% decrease in the average fluorescence lifetime of Cy5, confirming that it too is quenched by the sequential placement of the next acceptor. The low emission intensity from Cy5.5 in position 3 of the QD-wire (see Figure 5B,C) in conjunction with spectral overlap and cross-talk from the emission of the Cy5 donor did not allow us to isolate sufficient signal to analyze changes in the Cy5.5 lifetime when quenched by Cy7.

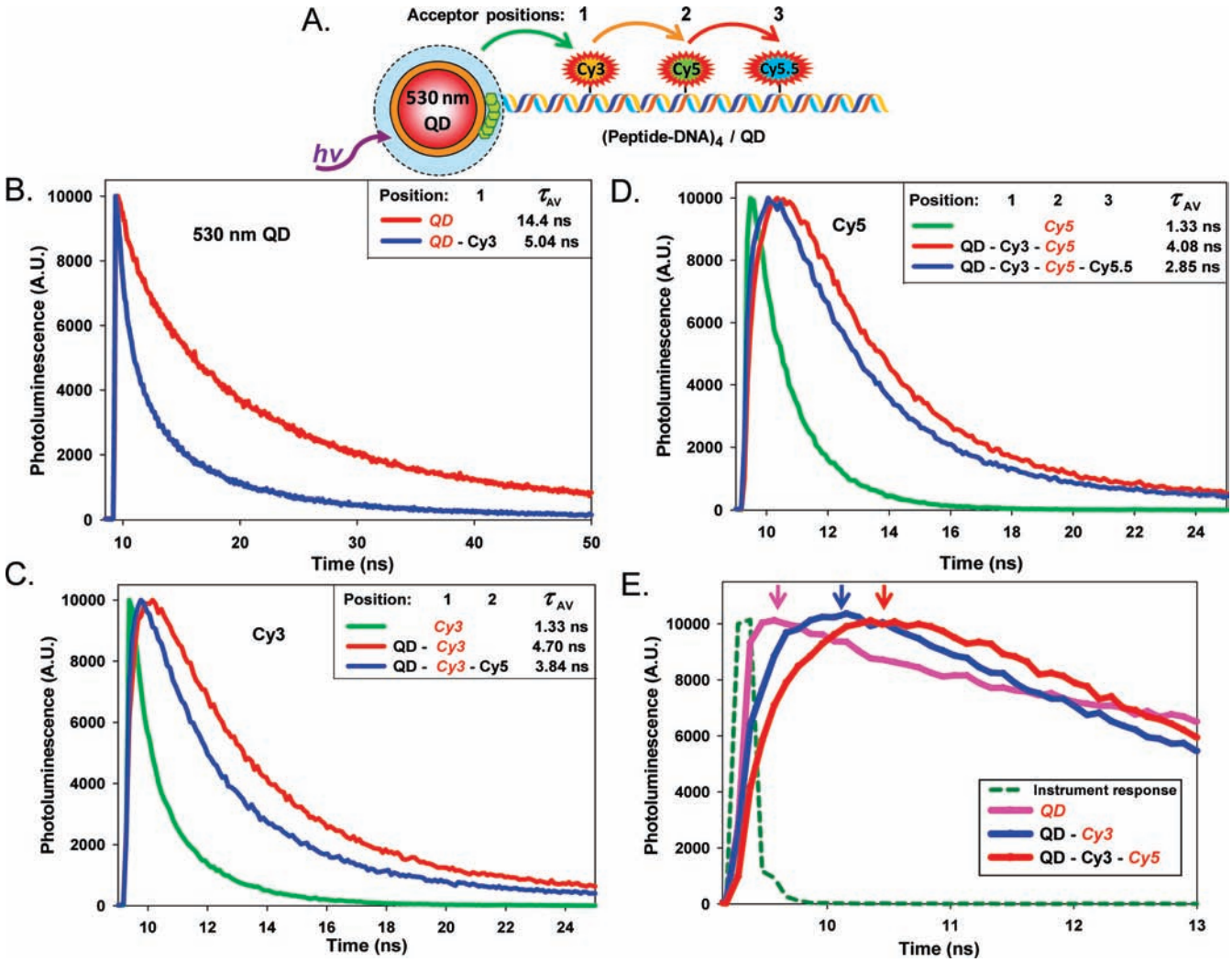

Figure 6. Time-resolved fluorescent data. (A) Schematic of the configurations interrogated consisting of 530 nm QDs self-assembled with 4 $(His)_6$−peptide−DNA samples hybridized with Cy3 in 1/Cy5 in 2/Cy5.5 in 3. (B) Plot of 530 nm QD PL intensity versus time in the absence (unlabeled DNA only) and presence of Cy3 acceptor DNA hybridized in position-1. (C) Plot of Cy3 PL intensity versus time for Cy3 DNA only, Cy3 acceptor DNA when hybridized in position-1 on a QD, and when Cy5 is added in position-2. (D) Plot of Cy5 PL intensity versus time for Cy5 DNA only, Cy5 acceptor DNA when hybridized in position-2 on a QD with Cy3 in position 1, and when Cy5.5 is added in position-3. (E) Plots highlighting increasing delays in the initial rise time for each of the indicated configurations. Red italics in each legend indicate the QD or dye-acceptor being monitored in that configuration. Colored arrows indicate the approximate apex of each experimental rise time.

An increase in the rise time of the signal was also observed as each acceptor was sequentially added to the DNA chain (see Figure 6E). In an ideal system where the excitation energy is absorbed exclusively by a single-primary donor, the rise time for each consecutive acceptor is determined by the excited state lifetime of the adjacent donor preceding it along the wire. Under these conditions, the rise time for each sequential acceptor will necessarily be equal to, or longer than, the previous acceptor rise time. This is an essential characteristic of sensitized, stepwise excitation. Rise time behavior in our system for the first set of FRET interactions was analyzed and compared to a modeling of the ET steps to provide additional insight into the underlying processes. Analysis of the rise times of the individual components in a multicomponent molecular complex that displays multiple-step energy transfer behavior is, however, significantly more complicated than that of traditional two-component systems. The rise time profile of the fluorescence signal is determined by a combination of the excitation function, the decay constants of the component(s) of the excited state complex along with the energy transfer rates, both to, and from each component.[17] For modeling, the kinetics of the stepwise energy transfer process from the initial QD donor to the Cy5 acceptor can be described by the following rate constant expressions:

$$k_{\text{QD*-Cy3-Cy5}} = (-k_{\text{QD}} - k_{\text{ETQD-Cy3}} - k_{\text{ETQD-Cy5}}) \quad (9)$$

$$k_{\text{QD-Cy3*-Cy5}} = (-k_{\text{Cy3}} + k_{\text{ETQD-Cy3}} - k_{\text{ETCy3-Cy5}}) \quad (10)$$

$$k_{\text{QD-Cy3-Cy5*}} = (-k_{\text{Cy5}} + k_{\text{ETCy3-Cy5}} + k_{\text{ETQD-Cy5}}) \quad (11)$$

The composite decay rate constant, $k_{\text{QD*-Cy3-Cy5}}$, characterizes the excited state population of the QDs in the QD−DNA Cy3-Cy5 nanowire. The measured decay characteristics of the unlabeled QD−DNA nanowire were used to determine k_{QD}; $k_{\text{ETQD-Cy3}}$ is the energy transfer rate constant from QD* to Cy3 obtained from measurement of the fluorescence decay from the QD-DNA-Cy3 nanowire without the Cy5 component and $k_{\text{ETQD-}}$

Table 3. Estimated Energy Transfer Rates and Rise Time Values

Fluorophore /configuration[a] Position: 1 2	τ_{Avg} (ns)[b]	$1/\tau$ (ns^{-1})	$k_{energy\ transfer\ rates}$ (ns^{-1})[c]	Efficiency	Rise times (ns)
530 nm QD	14.4	0.069			0.05
Cy3	1.33	0.752			
Cy5	1.33	0.752			
530 nm *QD* - Cy3	5.04	0.198	0.130 (QD*→Cy3)	65%	
530 nm QD - *Cy3*	4.70	0.213			0.34
530 nm QD - *Cy3* - Cy5	3.85	0.260	0.047 (Cy3*→Cy5)	18%	
530 nm QD - Cy3 - *Cy5*	4.08	0.245			0.93

[a] Red italics indicate fluorophore being interrogated in the configuration. [b] τ_{Avg}, average excited state lifetime. [c] Derived from lifetime data as described.

Cy5 is the energy transfer rate from QD* to Cy5. In eq 10, *k*ETQD-Cy3 is a growth term that reflects sensitized excitation by the excited state QDs. Similarly, in eq 11, *k*ETCy3-Cy5 is a growth term arising from sensitization by excited state Cy3. The rate constants for Cy3 and Cy5 were obtained from the measured fluorescence signals by fitting the tails of the fluorescence decays to two- or three-exponential decay functions and determining the average lifetime, $k = 1/\tau$avg, see Figure 6B−D. A detailed description of the modeling process is provided in the Supporting Information. The decay parameters used for the modeling are summarized in Table 3, and representative modeled temporal profiles for the sensitized emission contributions from the QD−DNA nanowire configurations are shown in Supporting Figure 2. Modeling predicted QD-sensitized rise times of ~3.5 ns for Cy3 and ~5 ns for Cy5, which are significantly longer that the observed rise times of 0.34 ns and 0.93 ns for Cy3 and Cy5, respectively.

On the basis of extinction coefficients at 300 nm and the stoichiometry of the QD-Cy3-Cy5 nanowire complex, we estimate that 51% of the laser pulse is absorbed by the QDs while 23% and 26% is absorbed directly by Cy3 and Cy5, respectively. The experimentally measured rise time curves thus represent a composite temporal behavior that includes significant contributions from directly excited Cy3 and Cy5 and excitation sensitized by energy transfer from the QD to Cy3 and Cy3 to Cy5. Contributions from directly excited Cy3/Cy5 significantly shorten the rise times from those predicted on the basis of sensitized emission only. Using an alternate laser source emitting between 370 and 410 nm would help avoid direct excitation of the dyes. The distribution of excited states in the same nanowire arising from both direct and sensitized excitation was estimated using a photon accounting spreadsheet (Supporting Table 2). Results here predict the fraction of QD-sensitized Cy3 and Cy5 to be 0.3 and 0.06, respectively, which correlates quite well with the 25% and 5.3% observed experimentally (Table 2).

Conclusions

There is intense interest in utilizing QD structures and ET for funneling in light-harvesting structures and this has even been demonstrated using a combination of QDs of variable size.[50,51] Preliminary structures combining QDs with DNA and dye acceptors have been described. Niemeyer constructed a three-chromophore FRET system consisting of a QD, enhanced yellow fluorescent proteins and Atto647-dye-modified oligonucleotides.[52] The intrinsic advantages of using QDs as the donor in this multiacceptor configuration enabled long-range FRET to be achieved over distances approaching 13 nm. Wang examined streptavidin-functionalized QDs decorated with biotinylated DNA that had been prelabeled with BOBO-3 intercalating dye.[53] Similar to our results, this dye functioned primarily as a QD quencher demonstrating minimal sensitized emission. Although elegant, these studies did not fully explore the potential of QDs as a donor specifically in photonic wire configurations. Significant differences in structure (hybrid QD-multiwire vs single-linear wire) make direct comparison between our assemblies and other photonic wire constructs difficult. The size of the QDs (radius = 28 Å) combined with that of the peptido-hydrazone linkage (~28 Å) and the DNA wire itself (132 Å) suggests that the FRET cascades proceeds outward from the central QD over distances of around 180 Å. Considering 4 or more DNA wires that are attached to opposite sides of the QD surface suggests photonically active structures demonstrating multiple ET cascades that can approach ~360 Å in diameter.

Here we use a bottom-up approach that includes synthesizing the QDs along with modifying the DNA with peptides to display multiple photonic wires around a single central QD donor. This approach allows access to novel structural and photophysical properties that can augment function. Some of the benefits uniquely available in this architecture are derived from the DNA's rigidity which extends the dyes outward from the central QD. For example, in Figure 5 the composite structure consists of a star-shaped assembly with 4 DNA wires extending radially from a central light harvesting QD donor. This in essence mimics a light harvesting dendrimer structure, although in this case the construct consists of many different types of molecules working in concert. Each of the 4 DNA strands, centrosymmetrically oriented with respect to the QD, hosts 4 acceptor fluorophores at well-defined positions with increasing distances from the QD. Although the dye-distances relative to the QD are fixed here, they can be varied on each DNA strand used or placed in different arrangements or orders. Previous studies have shown that on average 50 ± 10 peptides can be assembled to these QDs;[54] thus the number of DNA strands and/or dye acceptors can be significantly increased as desired. This also suggests the possibility of attaching more complex 3-dimensional DNA structures to the QDs beyond linear arrangements. It is important to reiterate that these possibilities are all available via self-assembly rather than covalent chemistry (peptide−DNA coordination to QD and DNA hybridization), which greatly facilitates applicability. Self-assembly also allows these photonic

(50) Franzl, T.; Shavel, A.; Rogach, A. L.; Gaponik, N.; Klar, T. A.; Eychmuller, A.; Feldmann, J. *Small* **2005**, *4*, 392–395.
(51) Rogach, A. L.; Klar, T. A.; Lupton, J. M.; Meijerink, A.; Feldmann, J. *J. Mater. Chem.* **2009**, *9*, 1208–1221.
(52) Lu, H.; Schops, O.; Woggon, U.; Niemeyer, C. M. *J. Am. Chem. Soc.* **2008**, *130*, 4815–4827.
(53) Lim, T. C.; Bailey, V. J.; Ho, Y. P.; Wang, T. H. *Nanotechnology* **2008**, *19*, 075701.
(54) Prasuhn, D. E.; Deschamps, J. R.; Susumu, K.; Stewart, M. A.; Boeneman, K.; Blanco- Canosa, J. B.; Dawson, P. E.; Medintz, I. L. *Small* **2009**, *6*, 555–564.

wires to be rapidly reconfigured by substituting different dye-labeled DNA strands or changing dye positions within strands.

Photophysically, we find that utilizing the QDs to harvest light in the UV and then emit in the visible portion can provide increased ET flows through these systems to the near IR as amply demonstrated by direct comparison of similar 4-fluorophore structures with and without the QD as donor in Figure 5C,D. The large absorption cross section of QDs combined with the ability to be excited in the UV makes for unique and potent donors in this role. It is anticipated that the exact mechanism(s) responsible for augmented FRET will be dissected using more refined constructs in forthcoming studies. The major impediments to higher efficiency energy flow in the structures examined here include the low QY of the organic dyes following sensitization and direct excitation of the organic dye acceptors. Options are available to address this including optimizing placement of the dyes on the DNA to engage in higher efficiency ET and the use of an excitation wavelength that minimizes direct excitation of the acceptors. Although the dyes were placed at distances slightly less than their R_0 values, the current results suggest that far closer positioning ($r \leq 0.5R_0$) would be more effective. Substitution of dyes manifesting higher QYs and larger extinction coefficients may also augment ET along with utilizing QDs that also display higher QYs themselves. Another possibility derives from the unique properties of the DNA architecture itself and that is having multiple donors interact with fewer acceptors, essentially the converse configuration to what we demonstrate. Although not focused on here, the same multifluorophore FRET configurations can also function as spectral barcodes where the intensity of each fluorophore is modulated to alter the code.[55,56] Using this simple example, with 5 fluorophores (QD plus 4 dyes) at just three different FRET-modulated intensities per fluorophore, 242 possible codes are possible (m colors at n intensities yields $n^m - 1$ codes). This may provide FRET-based codes and computing capacity as an alternative to the electrochemical-based QD coding recently characterized.[15,55] It is important to note that the structures assembled here represent only a tiny fraction of the possible architectural nanospace available for exploration when combining DNA, nanoparticles such as QDs, dyes, and hybrid peptido−DNA chemistries and far more versatile photonic structures can be expected in the future.

Acknowledgment. The authors acknowledge the CB Directorate/Physical S&T Division (DTRA), ONR, NRL and the NRL-NSI for financial support. K.B. and D.E.P. acknowledge ASEE fellowships through NRL. J.B.B.-C acknowledges a Marie Curie IOF.

Supporting Information Available: DHLA-ligand structure, dye structures, amine modification to the DNA, lifetime data, measurement parameters, modeling data, and selected discussion of results. This material is available free of charge via the Internet at http://pubs.acs.org.

JA106465X

(55) Medintz, I. L.; Farrell, D.; Susumu, K.; Trammell, S. A.; Deschamps, J. R.; Brunel, F. M.; Dawson, P. E.; Mattoussi, H. *Anal. Chem.* **2009**, *81*, 4831–4839.
(56) Han, M.; Gao, X.; Su, J. Z.; Nie, S. *Nat. Biotechnol.* **2001**, *19*, 631–635.